Porokeratotic Eccrine Nevus May Be Caused by Somatic Connexin26 Mutations

Jennifer A. Easton[1,2,7], Steven Donnelly[3,7], Miriam A.F. Kamps[1,2], Peter M. Steijlen[1,2], Patricia E. Martin[3], Gianluca Tadini[4], René Janssens[5], Rudolf Happle[6], Michel van Geel[1,2] and Maurice A.M. van Steensel[1,2]

Porokeratotic eccrine ostial and dermal duct nevus, or porokeratotic eccrine nevus (PEN), is a hyperkeratotic epidermal nevus. Several cases of widespread involvement have been reported, including one in association with the keratitis–ichthyosis–deafness (KID) syndrome (OMIM #148210), a rare disorder caused by mutations in the *GJB2* gene coding for the gap junction protein connexin26 (Cx26). The molecular cause is, as yet, unknown. We have noted that PEN histopathology is shared by KID. The clinical appearance of PEN can resemble that of KID syndrome. Furthermore, a recent report of cutaneous mosaicism for a *GJB2* mutation associated with KID describes linear hyperkeratotic skin lesions that might be consistent with PEN. From this, we hypothesized that PEN might be caused by Cx26 mutations associated with KID or similar gap junction disorders. Thus, we analyzed the *GJB2* gene in skin samples from two patients referred with generalized PEN. In both, we found *GJB2* mutations in the PEN lesions but not in unaffected skin or peripheral blood. One mutation was already known to cause the KID syndrome, and the other had not been previously associated with skin symptoms. We provide extensive functional data to support its pathogenicity. We conclude that PEN may be caused by mosaic *GJB2* mutations.

Journal of Investigative Dermatology (2012) **132,** 2184–2191; doi:10.1038/jid.2012.143; published online 17 May 2012

INTRODUCTION

The term ''porokeratotic eccrine ostial and dermal duct nevus'' was first used by Abell and Read (1980) to describe a hard, verrucous epidermal nevus. Histopathological features typically include ortho- or parakeratotic plugs protruding from dilated (eccrine) ducts and follicular openings. Depending on sectioning, these plugs can appear as so-called cornoid lamellae. In addition, hyper(para)keratosis and wavy psoriasiform epidermal acanthosis can also be present (Aloi and Pippione, 1986). Comedo-like or spiky lesions can be prominent in porokeratotic eccrine nevus (PEN) when located on the palms or soles (Sassmannshausen *et al.*, 2000). Several cases of bilaterally systematized lesions of PEN affecting large areas of the body have been reported (Cobb *et al.*, 1990; Kroumpouzos *et al.*, 1999; Cambiaghi *et al.*, 2007; Goddard *et al.*, 2009). Happle and Rogers (2002) recently proposed the more compact designation ''PEN''.

The molecular cause is, as yet, still unknown. However, we have noted that the characteristic cutaneous histopathology is shared by the keratitis–ichthyosis–deafness (KID) syndrome (OMIM #148210). This rare disorder is caused by mutations in the *GJB2* gene coding for the gap junction protein connexin26 (Cx26; van Steensel *et al.*, 2002). KID syndrome histopathology typically shows dilated follicular and eccrine duct openings with a preserved granular layer and ortho-/parakeratotic plugs that can appear as cornoid lamellae. The epidermis shows wavy psoriasiform acanthosis. Clinically, the ichthyosis in KID is characterized by generalized figurate erythema and cobblestone-like or spiky hyperkeratosis (de Zwart-Storm *et al.*, 2009). Thus, KID syndrome can appear as a generalized form of PEN. Two of the authors (PS and RH) have personally seen a newborn with lethal KID syndrome born to a women diagnosed with PEN. They initially diagnosed the child with ''generalized PEN'', which was later revised (Steijlen P, personal communication). Titeux *et al.* (2009) recently described mosaicism for a Cx26 mutation causing the previously reported substitution p.Asp50Asn (D50N) in the mother of a child with KID syndrome. The mother had a short stature and bilateral linear

[1]*Department of Dermatology, Maastricht University Medical Center, Maastricht, The Netherlands;* [2]*GROW School for Oncology and Developmental Biology, University of Maastricht, Maastricht, The Netherlands;* [3]*Department of Life Sciences, School of Health and Life Sciences, Glasgow Caledonian University, Glasgow, UK;* [4]*Institute of Dermatological Sciences, School of Medicine and Surgery and Post Graduate School of Dermatology and Venereology, University of Milan, Milan, Italy;* [5]*Department of Dermatology, Jeroen Bosch Ziekenhuis, 's Hertogenbosch, The Netherlands and* [6]*Department of Dermatology, Freiburg University Medical Center, Freiburg, Germany*

[7]*These authors contributed equally to this work.*

Correspondence: Jennifer A. Easton, Department of Dermatology, Maastricht University Medical Center, Maastricht, The Netherlands.
E-mail: jennifer.easton@maastrichtuniversity.nl

Abbreviations: CK10, cytokeratin10; Cx26, connexin26; ERGIC, endoplasmic reticulum–Golgi intermediate compartment; KID, keratitis–ichthyosis–deafness; PEN, porokeratotic eccrine nevus

Received 1 June 2011; revised 9 February 2012; accepted 6 March 2012; published online 17 May 2012

hyperkeratotic skin lesions on the trunk. Unfortunately, the photographs provided in that report were of insufficient quality to confidently make a diagnosis, but the abnormalities might be consistent with PEN. Finally, cases of nonsegmental KID syndrome were recently reported to be ''associated with PEN'', on the grounds of purely histopathological findings (Criscione *et al.*, 2010; Lazic *et al.*, 2011). Considering the above, we hypothesized that PEN might be caused by Cx26 mutations associated with KID syndrome or similar hyperkeratotic gap junction disorders (de Zwart-Storm *et al.*, 2009). Thus, we analyzed the *GJB2* gene in skin and blood samples from two patients who were referred with widespread PEN, confirmed by histopathological examination (Figure 1). Both patients were otherwise healthy and had no other symptoms besides skin lesions.

RESULTS

Case reports

Clinical examination of patient 1, from Italy, showed widespread spiky hyperkeratotic papules and plaques with linear distribution on the extremities, and mostly diffuse palmoplantar involvement (Figure 1a–c). The nails of both hands and the left foot were dystrophic. The abnormalities had been present since birth and were not progressive. There were no mucosal abnormalities. Hair and teeth were normal. There was no hearing loss, and family history was negative. Several biopsies were taken from affected sites and sent for histopathological examination. All showed abnormalities that were deemed consistent with PEN (Figure 1i–j). Patient 2, from the Netherlands, had less widespread involvement, presenting with linear spiky hyperkeratotic plaques on both feet and geographic brown-red plaques with a sharply demarcated border in a linear distribution on the trunk and proximal extremities (Figure 1d–f). The skin lesions had been present all his life and were not progressive. Hearing loss was not present. Family history was negative. A biopsy taken from the trunk showed similar abnormalities to those in patient 1 (Figure 1k and l). Both patients were diagnosed as having PEN.

Mutation analysis indicates somatic mosaicism

In both patients, we detected mutations within the *GJB2* gene in samples from all biopsied disease sites. Specifically, three sites were sampled in patient 1 (foot sole, knee, and trunk) and two sites in patient 2 (axilla and trunk). We could only amplify wild-type (WT) *GJB2* from unaffected skin (one sample per patient, Figure 2a and b) and peripheral blood leukocytes (not shown). Patient 1 had a transition c.40A>T (Figure 2a) causing the known KID-associated amino acid change p.Asn14Tyr (N14Y, Arita *et al.*, 2006); patient 2 had a transversion c.279G>A (Figure 2b) causing the substitution p.Met93Ile (M93I). We also sequenced the *GJB6* gene, as there are reports suggesting that mutations in *GJB6* can cause disorders resembling those associated with *GJB2* (Jan *et al.*, 2004). No *GJB6* mutations were found in either patients. Although N14Y is known to be pathogenic (Arita *et al.*, 2006; de Zwart-Storm *et al.*, 2011),

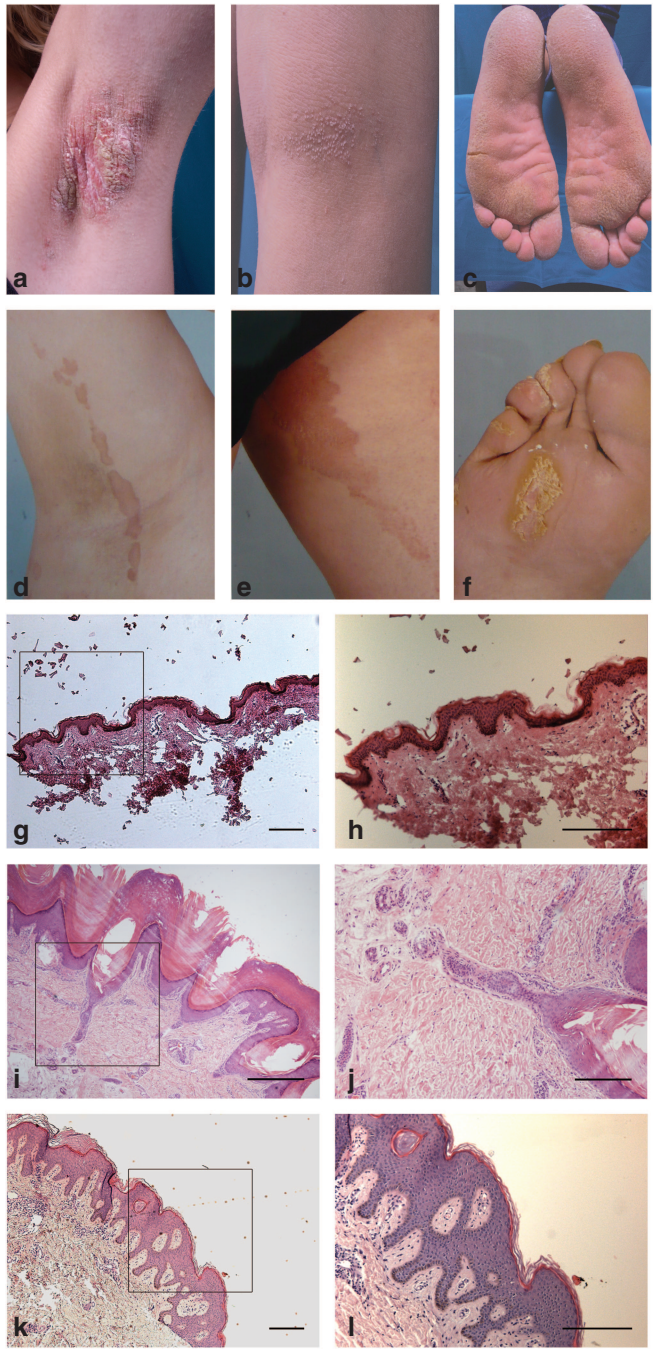

Figure 1. Clinical and histopathological phenotypes. Phenotype of patient 1, showing circumscript spiky hyperkeratosis with linear distribution in the axilla (**a**) and knee flexure (**b**). The feet are more diffusely affected (**c**). Phenotype of patient 2, showing linear hyperkeratotic plaques with spiky surface on the foot (**f**) and linear, sharply demarcated geographic plaques elsewhere with a smooth surface (**d**, **e**). Histopathology is shown in panels **g**–**l**. Normal skin section shown in **g** (×5) and **h** (×10). Biopsy taken from the foot of patient 1 (**i**, ×10; **j**, ×100) shows a dilated eccrine duct with parakeratotic lamellae (**i**, **j**); sample from the trunk taken from the Dutch patient (**k**, ×5; **l** ×10) shows wavy epidermis with psoriasisform acanthosis and basket-weave hyperkeratosis. Marked square area denotes magnified area for **h**, **j**, **k**. Bar = 300 μm (except **j** = 30 μm).

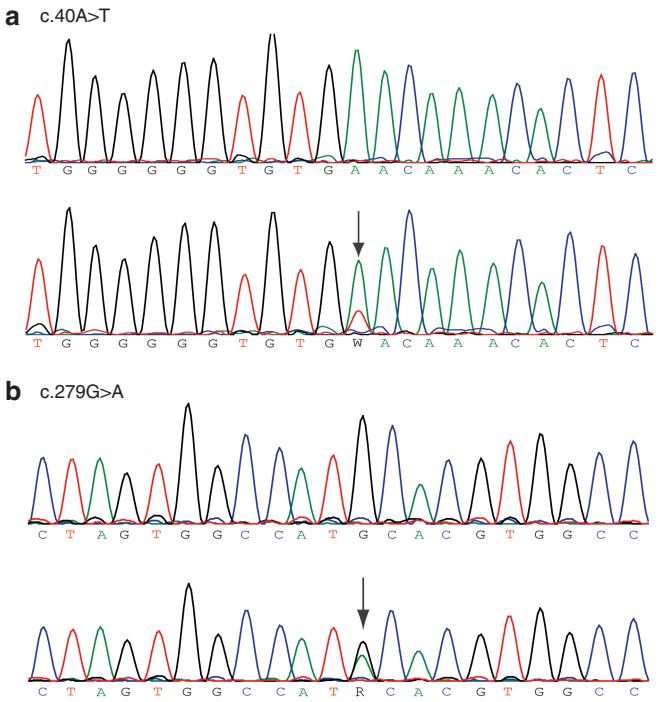

Figure 2. Sequence traces showing the presence of *GJB2* mutations (arrows) in lesional (bottom panels) but not in unaffected skin (top panels). Patient 1 has a transition c.40A>T mutation (N14Y) (**a**), whereas patient 2 presents with a transversion c.279G>A mutation (M93I) (**b**). Reduced peak height at mutation point is indicative of mosaicism.

M93I has not previously been reported in conjunction with cutaneous abnormalities.

We performed additional investigations to determine whether M93I is a pathogenic change.

Affected skin shows hyperproliferation and altered Cx26 expression patterns

Skin biopsies from the two patients were stained for Cx26 plus a number of cell proliferation/differentiation markers and compared with normal skin tissue (Figure 3). In both normal tissue (Figure 3a) and N14Y patient tissue (Figure 3b), Cx26 was observed in the cornified layer as well as within the spinous and granular layers. The pattern in normal skin is consistent with previous reports (Richard *et al.*, 2002). Within the M93I patient tissue (Figure 3c), however, Cx26 expression was only observed within the spinous and granular layers and not in the cornified layer. In control skin, Cx26 staining has a dense punctate distribution, at points of cell-to-cell contact. Biopsies from the patient harboring the N14Y mutation, in contrast, displayed a more dispersed punctate pattern of staining. Interestingly, M93I expression is intermediate, the staining being accentuated in certain membrane localizations. Expression of cytokeratin10 (CK10), an early differentiation marker, was greatly increased in both N14Y and M93I patient tissues in comparison with normal tissue, as was loricrin expression (a marker of terminal differentiation). To determine whether the N14Y and M93I mutations resulted in an increase in cellular proliferation, tissues were stained with Ki67. In addition, tissues were co-stained with the basal cell marker CK14. Ki67+ cells were present within the basal layer of normal and patient tissue; however, the percentage of Ki67+/CK14+ cells was increased in both patient tissue samples. In normal tissue, 19.1% (±1.87% SEM) cells had double-positive staining, whereas patient 1 had 25.7% (±6.3% SEM) and patient 2 had 26.5% (±5.8% SEM). These differences were not found to be statistically significant.

M93I-GFP traffics to the cell membrane and forms large gap junction plaques

HeLa Ohio cells (which do not express endogenous connexins) were transfected with Cx26WT-mCherry alone (Figure 4a), M93I-GFP alone (Figure 4b), or both Cx26WT-mCherry and M93I-GFP (Figure 4c). As with Cx26WT-mCherry expression, M93I-GFP was observed both at the plasma membrane and within the cytoplasm as intracellular stores. Co-transfection of Cx26WT-mCherry with M93I-GFP showed clear co-localization. From this, we concluded that the M93I mutation does not disrupt interaction with Cx26WT. In addition, M93I-GFP formed large gap junction plaques at points of cell-to-cell contact, highly separated from intracellular regions as denoted by co-staining with the endoplasmic reticulum–Golgi intermediate compartment (ERGIC) marker p58 (Figure 5b). We can conclude from this that the M93I mutation has no adverse effect on trafficking, unlike the D66H mutation, which remains trapped in intracellular areas (Figure 5c).

Junctional functionality measured by dye transfer is not affected by the M93I mutation

As aberrant connexin signaling is associated with a range of Cx26-related disorders, we assessed the ability of M93I-GFP to form functional gap junctions and hemichannels. A variety of assays are widely used to determine gap junction coupling efficiency. These include microinjection analysis, in which coupling efficiency is determined by the extent of transfer of small fluorescent dyes of differing charge and mass (e.g., Easton *et al.*, 2009), and parachute assays, which determine the transfer of the fluorescent probe calcein AM (molecular weight = 623 Da, charge −4). The latter have been widely used by ourselves and others in the field (Ziambaras *et al.*, 1998; Dürig *et al.*, 2000; Rudkin *et al.*, 2002). In the present work, we performed parachute assays between HeLa Ohio cells transfected with the different complementary DNA constructs and HeLa26 cells that stably express Cx26 (Figure 6a). In this case, it is evident that both untransfected HeLa Ohio cells and those transfected to express D66H-GFP were unable to form functional gap junction channels, as can be seen by the restricted spread of calcein to adjoining cells (Figure 6a). By contrast, cells transfected with either Cx26WT-GFP or M93I-GFP were able to transfer dye to HeLa26 cells, illustrating formation of functional gap junction channels by the M93I mutations. There was no statistically significant difference between the two groupings (Figure 6b). We can be certain that the observed dye transfer is due to channel formation between the transfected HeLa Ohio cells and the HeLa26 cells, because both non-transfected HeLa Ohio cells and those transfected with D66H-GFP

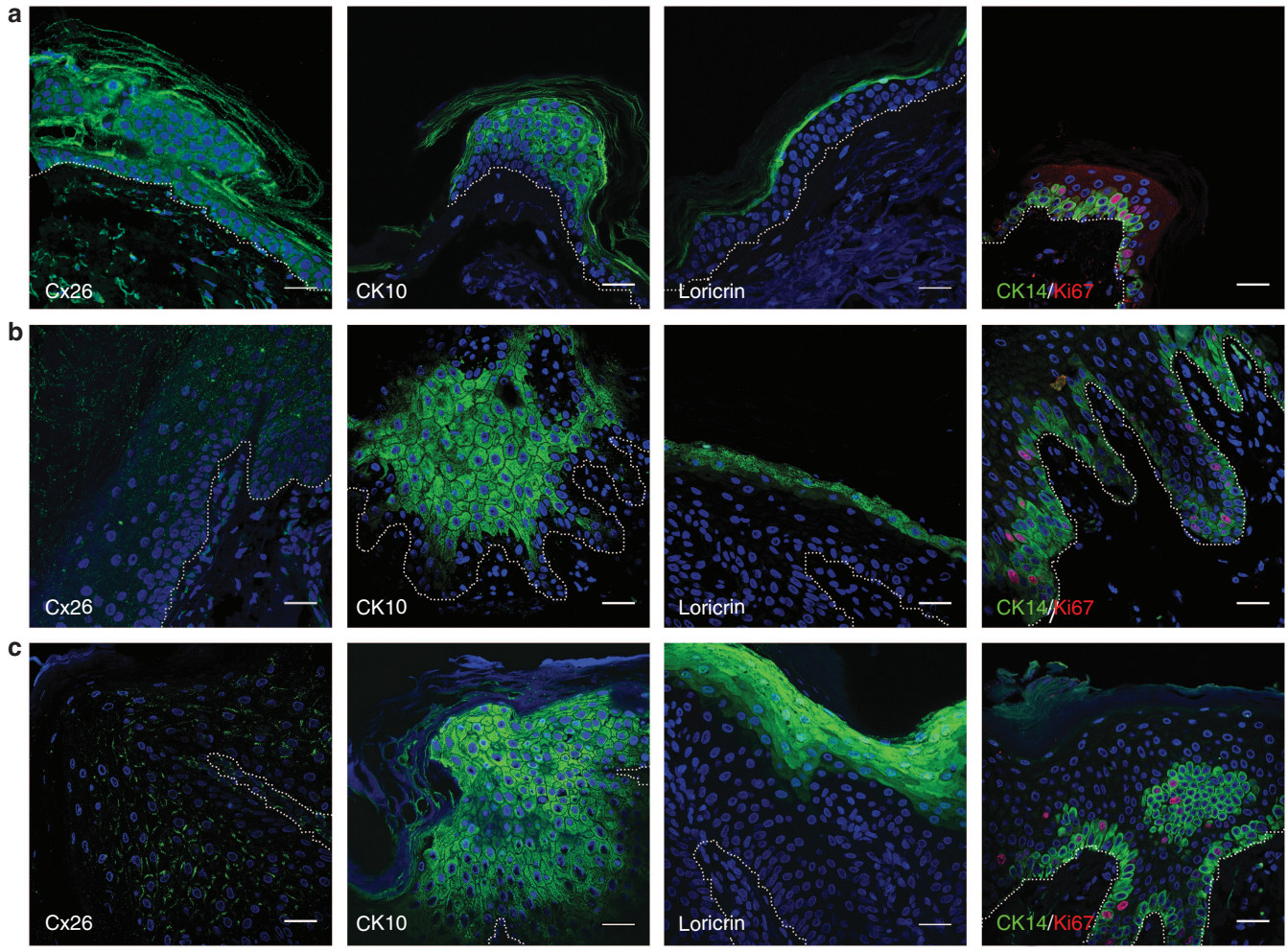

Figure 3. Immunohistological comparison of normal and patient tissue. Tissue sections from normal (**a**), patient 1 (**b**), and patient 2 (**c**) skin were stained with connexin26 (Cx26), cytokeratin10 (CK10), and loricrin (all green). In addition, tissue was co-stained with Ki67 (red) and CK14 (green) to identify proliferating cells in the basal layer. Nuclei stained with 4′-6-diamidino-2-phenylindole. Patient skin shows a clear increase in CK10 and loricrin staining plus an increase in Ki67-positive cells in the basal layer. Interestingly, no Cx26 staining was observed in the stratum corneum of patient 2. For both patients, overall Cx26 staining seems to be less intense than that of wild type (**a**). In addition, patient 2 (M93I) shows plaque formation, in contrast to patient 1 (N14Y). For orientation purposes, the basal layer is indicated by a dotted white line. Bar = 30 μm.

(associated with Vohwinkel's syndrome and known to be nonfunctional) showed no transfer.

In addition to the ability to form functional gap junctions, we investigated the effect of M93I-GFP expression on hemichannel signaling. Exposing connexins to zero calcium conditions is a robust method to induce hemichannel openings that can be monitored by ATP release and subsequently blocked by a range of connexin hemichannel blockers (Leybaert *et al.*, 2003). In HeLa Ohio cells transfected to express a control vector (GFP) or the Cx26 mutation D66H-GFP, no ATP release was detected following the calcium switch. By contrast, in cells transfected with Cx26WT-GFP or M93I-GFP, a significant release in ATP was observed, which was blocked upon co-incubation with the hemichannel blocker carbenoxolone (Figure 6c). Measured ATP release was lower in M93I-GFP-expressing cells than was observed for those expressing Cx26WT-GFP, although this was not statistically significant.

DISCUSSION

On the basis of our experimental findings, we suggest that PEN can be associated with somatic mutations in *GJB2* coding for the gap junction protein Cx26. We found two distinct amino acid substitutions in two unrelated patients. One mutation, N14Y, is a known pathogenic change that has been reported in conjunction with disorders resembling the KID syndrome (Arita *et al.*, 2006; de Zwart-Storm *et al.*, 2011). The second mutation, M93I, has been previously reported in *trans* with the deafness-associated truncating mutation c.del35G (Wu *et al.*, 2002). It is not clear from that report whether or not that particular patient had skin symptoms. If not, the change may not have been pathogenic to the skin, or may have caused only very mild symptoms that were missed. Another, more intriguing, explanation might be that mutations in Cx26 associated with skin disease only cause symptoms in *trans* with a WT allele. The latter hypothesis would be consistent with the observation that

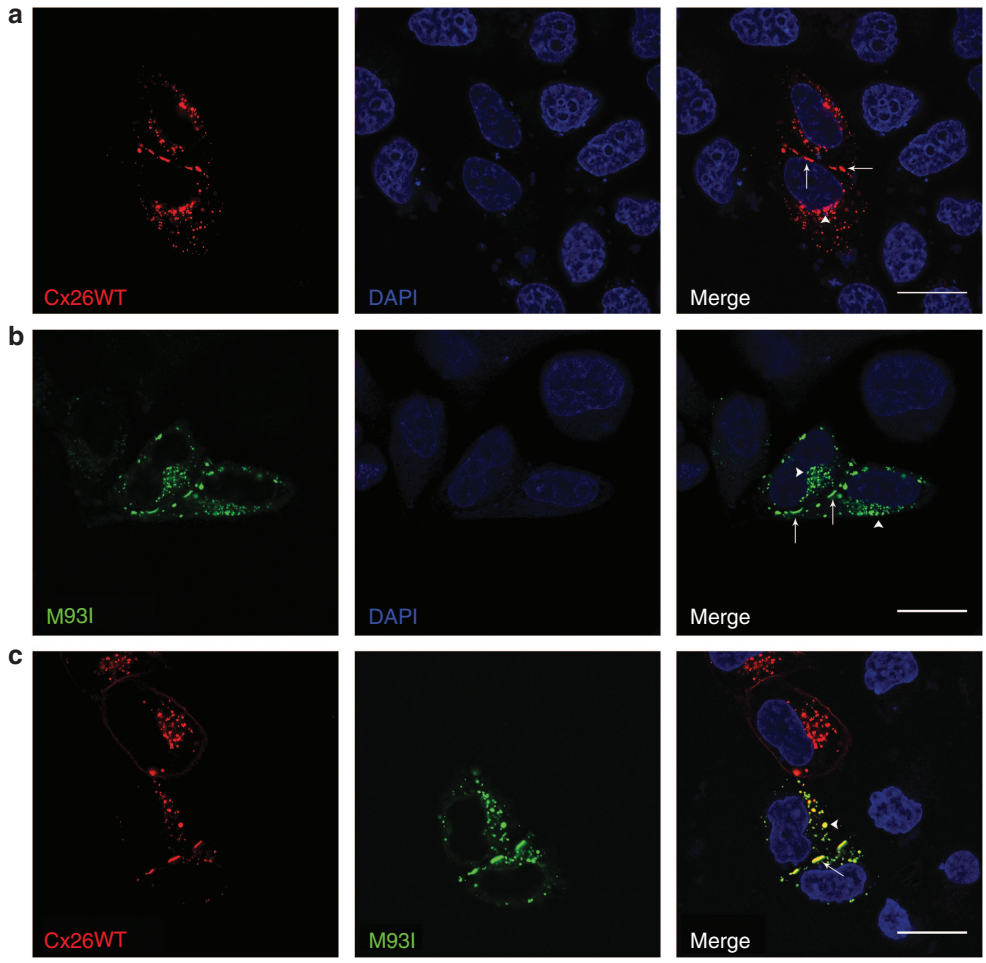

Figure 4. M93I-GFP traffics normally to the plasma membrane and co-localizes with Cx26WT-mCherry. HeLa Ohio cells were transfected with Cx26WT-mCherry (**a**, red), M93I-GFP (**b**, green), or both Cx26WT-mCherry and M93I-GFP (**c**), and protein localization was analyzed after 24 hours. In both single and double transfected cells, Cx26WT-mCherry and M93I-GFP expression was observed both within the cytoplasm (white arrow heads) and at the plasma membrane (white arrows), indicating cellular stores and connexin (Cx) trafficking to the membrane. Cx26WT-mCherry and M93I-GFP co-localized throughout the cell (yellow) and formed visible gap junction plaques at points of cell-to-cell contact. Nuclei are stained with 4′-6-diamidino-2-phenylindole (DAPI; blue). Bar = 20 μm.

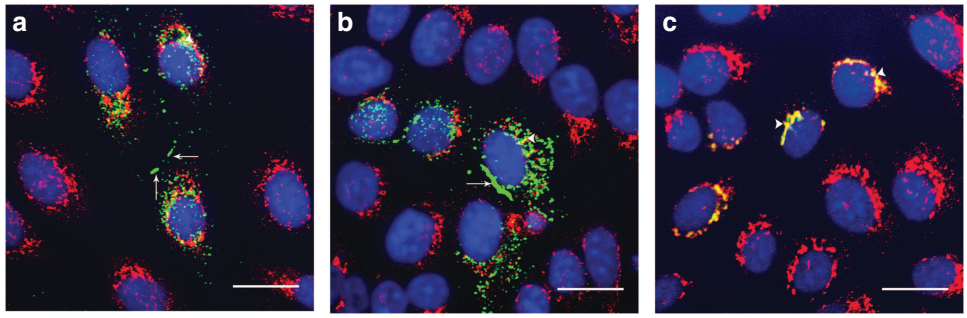

Figure 5. HeLa Ohio cells were transfected with Cx26WT-GFP, M93I-GFP, or D66H-GFP (green) and expression analyzed 24 hours post transfection. Cells were stained with the endoplasmic reticulum–Golgi intermediate compartment marker p58 (red). Co-localization of Cx26 protein with p58 was observed with all Cx26 transfectants (white arrow heads), indicative of intracellular stores and Cx trafficking pathways. Large gap junction plaques are clearly seen at points of cell-to-cell contact for both Cx26WT-GFP and M93I-GFP (**a** and **b**, respectively, white arrows). D66H-GFP was used as a control, as this is a Cx26 mutation known not to traffic; no gap junctions were observed in D66H-GFP-expressing cells (**c**). Nuclei stained with 4′-6-diamidino-2-phenylindole (blue). Bar = 20 μm.

mutations in Cx26 causing cutaneous symptoms are dominant. Previous observations of *trans*-dominant effects from mutant Cx26 on Cx43 also support this idea (Rouan *et al.*, 2001). It will be interesting to pursue this notion in future research. Our finding of the mutation in affected skin only and not in unaffected areas or peripheral blood further

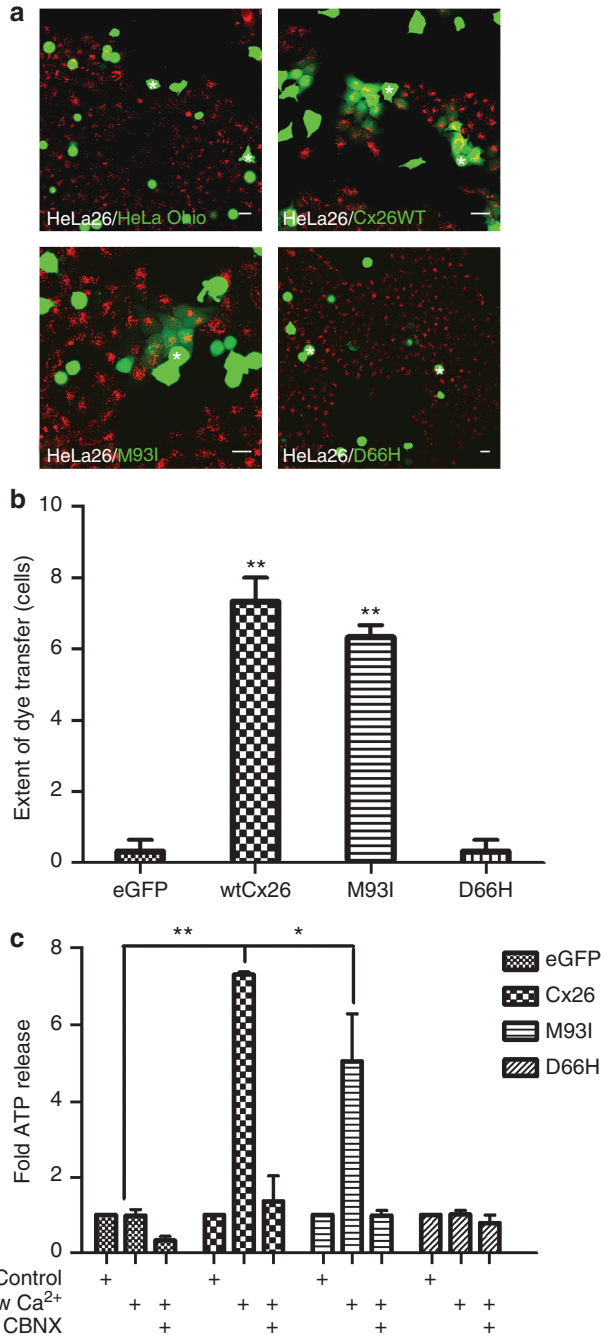

Figure 6. M93I-GFP forms functional gap junctions with Cx26WT. HeLa Ohio cells transfected with relevant complementary DNA constructs were layered onto a monolayer of HeLa26 cells labeled with DiLC (red) (**a**). Dye transfer was observed between HeLa Ohio cells transfected with either Cx26WT-GFP or M93I-GFP and HeLa26 cells, but not between cells transfected with GFP alone or D66H-GFP and HeLa26 cells. Bar = 20 μm. The number of cells a ''donor'' cell transferred dye to was calculated (**b**). In addition, hemichannel activity via ATP release was examined in HeLa Ohio cells transfected with GFP alone, Cx26WT-GFP, M93I-GFP, or D66H-GFP (**c**). Results were calculated as nM ATP released per μg of protein and are expressed as a fold increase in ATP release. $N = 3$, $^{**}P < 0.05$; $^{*}P < 0.01$.

argues in favor of its pathogenicity. To provide more pertinent proof, we conducted additional studies. Our experiments illustrate that M93I maintains many of the functional parameters of Cx26WT as measured by our assays. Unlike mutations associated with conditions such as Vohwinkel's syndrome, where the protein is restricted to intracellular locations and does not form hemichannels or gap junctions in homotypic conformations (Bakirtzis *et al.*, 2003; Marziano *et al.*, 2003), M93I targets to the cell membrane and forms both hemichannels and gap junctions. Our parachute assays demonstrate that M93I is able to form functional channels, in contrast to D66H. On the basis of calcein dye transfer, gap junctions composed of M93I have functional properties similar to Cx26WT, although it is possible that permeability to other dyes might be altered. We have previously demonstrated that alterations in the size of the dye do not correlate with disease severity (de Zwart-Storm *et al.*, 2008) and therefore decided not to pursue this particular property of gap junctions. The zero calcium switch experiment clearly illustrates that M93I retains the ability to form hemichannels. Aberrant or enhanced hemichannel activity has been implicated in the pathogenesis of KID syndrome (Lee *et al.*, 2009). Compared with Cx26WT, we find that, for M93I, ATP release upon zero calcium switching is marginally reduced. From this, we tentatively conclude that hemichannel behavior might be affected by mutation M93I, and other assays including electrophysiology comparisons may elucidate these changes further in the future. Importantly, immunofluorescence analysis of CK10 and Ki67 expression in affected skin from both patients clearly indicates increased keratinocyte proliferation, which is consistent with earlier reports describing epidermal hyperproliferation due to Cx26 mutations. The increased loricrin staining supports this interpretation. We also see altered spatial localization of Cx26 in patient samples (the antibody does not distinguish mutant from WT), and this may contribute to the pathogenesis of the disorder. It is noteworthy that the expression of both mutant forms is reduced, and M93I is no longer found in the stratum corneum as opposed to N14Y and WT. These differences between patients and controls likely cannot be ascribed to the biopsy site, as there are no significant regional variations in cutaneous Cx26 expression (Richard *et al.*, 2002).

At present, we do not know what consequences the altered epidermal Cx26 expression patterns have for skin function. However, our observations would suggest that loss of function resulting from reduced Cx26 levels might contribute to epidermal hyperproliferation. We note that M93I seems to still form gap junction plaques (Figure 3c), in contrast to N14Y (Figure 3b), which shows a more diffuse distribution consistent with lack of gap junction formation.

From the above data, we conclude that M93I is likely a pathogenic change, but expression of M93I does not impact Cx26 function as severely as N14Y expression, as measured by our assays. This might be reflected in the clinical presentation. Whereas the Italian patient had the hyperkeratotic skin changes typically observed in KID syndrome, the Dutch patient had altogether less pronounced lesions. It is conceivable that the less pronounced phenotype correlates with the milder impact of M93I on Cx26 function. The clinical differences are reflected in the histopathology,

which shows much milder abnormalities in the Dutch patient.

From our findings, we conclude that PEN could be caused by different somatic Cx26 mutations. There may be a genotype–phenotype correlation, and it will be of considerable interest to determine the causative mutation in further cases of PEN. Our findings also illustrate that our assays for Cx26 function do not always predict whether or not a mutation is pathogenic, raising questions as to the mechanism by which mutations in Cx26 cause disease and underscoring the need for analysis of patient material.

MATERIALS AND METHODS

Sequencing and site-directed mutagenesis

GJB2 WT gene was cloned into the vectors peGFP-N1 (BD Biosciences, Breda, The Netherlands) and pmCherry-N1 (Clontech, via Westburg BV, Leusden, The Netherlands) as previously reported (de Zwart-Storm *et al.*, 2007), yielding the constructs *GJB2*-GFP (coding for Cx26WT-GFP) and *GJB2*-mCherry (coding for Cx26WT-mCherry). Primer sequences used for *GJB2* cloning were 5′-gaattc GCCCAGAGTAGAAGATGGATTGG-3′ (forward, *Eco*RI adapter indicated in lowercase) and 5′-ggatccGCAACTGGCTTTTTTGACTTC-3′ (reverse, *Bam*HI adapter in lowercase). We then introduced the c.279G>A (M93I) mutation into the *GJB2*-GFP construct with site-directed mutagenesis using KOD proof-reading enzyme (Novagen, Merck BV, Schiphol-Rijk, The Netherlands), which yielded the construct *GJB2*(c.279G>A)-GFP (coding for Cx26(M93I)-GFP, termed M93I-GFP). Primer sequences were 5′-GCCAGCGCTCCTAGTGGC-CAT***A***CACGTGGCC-3′ (forward) and 5′-GTCTCCGGTAGGCCACG TG***T***ATGGCCACTAG-3′. Mismatched nucleotides are in boldface and italics. Clones were selected and checked as to whether they contained the mutation before transfection into cells. Patient DNA was isolated from 3-mm punch biopsies from which dermis was removed using the Qiagen Maxi-prep kit (Qiagen, Venlo, The Netherlands) according to the manufacturer's instructions. Sequencing was performed by LGC genomics. These studies are covered under an umbrella agreement that has been approved by the Maastricht University ethics committee, number: 06-1-035. As part of the agreement, we have permission to use patient samples for study purposes and express written consent is not necessary. Mutation analysis is performed in regular diagnostics services and is as such not subject to research agreements. The study conformed to the Declaration of Helsinki Principles.

Cells and cell culture

All cell lines were cultured at 37 °C in 5% CO_2. HeLa Ohio cells were maintained in DMEM (Lonza, Breda, The Netherlands) supplemented with 10% fetal calf serum and L-glutamine (2 mM). HeLa26 cells (HeLa Ohio cells stably transfected to express Cx26) were maintained in DMEM supplemented with 10% fetal calf serum, L-glutamine (2 mM), and puromycin (0.5 μg ml^{-1}).

For immunofluorescence studies, cells ($\sim 2 \times 10^5$) were cultured on 16-mm^2 glass coverslips (Fisher Scientific, Loughborough, UK) in 12-well, sterile tissue culture plates (Greiner Bio-One, Stonehouse, UK). For parachute assay, setup cells ($\sim 2 \times 10^5$) were cultured in 12-well, clear, sterile tissue culture plates. For ATP assay preparation, cells ($\sim 2 \times 10^3$) were cultured in 96-well, clear, sterile tissue culture plates (Greiner Bio-One).

Transfections

Cells were transfected for 24 hours with appropriate complementary DNA at 1 μg (12-well plate) or 0.2 μg. (96-well plate) using Lipofectamine 2000 according to the manufacturer's instructions (Invitrogen, Paisley, UK).

Immunohistochemistry

Skin sections were cut (10 μm) from paraffin-embedded biopsies of normal and patient tissue. Following antigen retrieval using citrate buffer, sections were stained with Cx26 (1:50, Invitrogen), CK10 and CK14 (neat, MuBio, Maastricht, The Netherlands), loricrin (1:400, Abcam, Cambridge, UK), and Ki67 (1:100, Leica, Valkenswaard, The Netherlands). Secondary antibodies used for single stains were either Rabbit anti-Mouse-FITC or Swine anti-Rabbit-FITC (1:100, Dako, Heverlee, Belgium) antibody. For double stains, Goat anti-Mouse-FITC and Goat anti-Rabbit-Texas Red (1:80, Southern Biotech, ITK Diagnostics, Uithoorn, The Netherlands) secondary antibodies were used. Nuclei were stained with 4′-6-diamidino-2-phenylindole (0.5 μg ml^{-1}). Sections were examined using a Leica confocal microscope. Images were analyzed using the ImageJ software (http://rsbweb.nih.gov/ij).

Immunofluorescence

The ERGIC was stained using anti-ERGIC-53/p58 (1:100, Sigma-Aldrich, Dorset, UK). Goat anti-Rabbit conjugated to Alexa 488 (Invitrogen) was used as the secondary antibody. The nuclei of the cells were stained blue using 4′-6-diamidino-2-phenylindole (2.5 μg ml^{-1}; Sigma-Aldrich). Slides were viewed on a Zeiss LSM 510 Meta confocal microscope (Carl Zeiss, Welwyn Garden City, UK). Images were analyzed using ImageJ.

Parachute assays

HeLa26 cells were stained with cell tracker cm-DIL (1 μg ml^{-1}; Invitrogen) for 5 minutes at 37 °C and then for 15 minutes at 4 °C. After staining, cells were washed thoroughly with phosphate-buffered saline. HeLa Ohio cells transfected with Cx26 constructs were loaded with calcein AM (2.5 μM; Invitrogen) by incubating at 37 °C in 5% CO_2 for 30 minutes. After thorough washing with phosphate-buffered saline, cells were trypsinized and seeded onto confluent monolayers of HeLa26 cells. Cells were incubated for ~5 hours, and dye transfer patterns were analyzed using a Zeiss LSM510 scanning confocal microscope. ImageJ was used to quantify the data (method adapted from Ziambaras *et al.*, 1998).

ATP assays

Cells were washed in phosphate-buffered saline and incubated in DMEM for 1 hour at 37 °C in 5% CO_2; to block hemichannel activity, cells were incubated for 1 hour in DMEM with 100 μM carbenoxelone. To determine hemichannel activity, cells were then challenged, for 2.5 minutes, with Ca^{2+}-free phosphate-buffered saline (calcium switch); DMEM was used for control cells. The media were then harvested and extracellular ATP levels immediately analyzed using a luciferin–luciferase assay (Sigma-Aldrich). Post challenge, cells were washed and harvested in 5% trichloroacetic acid. Experiments were performed in triplicate per setting and on at least three further occasions. Transfection efficiencies and relative Cx expression levels were monitored by virtue of GFP autofluorescence, real-time PCR, and western blot analysis to detect

Cx26 expression. Total protein was measured using the Bio-Rad Laboratories D_C protein assay kit (Bio-Rad Laboratories, Hemel Hempstead, UK) following the manufacturer's instructions. Results were then standardized against protein concentration and results presented as a fold change compared with the control (Wright *et al.*, 2012).

CONFLICT OF INTEREST

The authors state no conflict of interest.

ACKNOWLEDGMENTS

JAE is supported by the GROW School for Oncology and Developmental Biology. MAMvS is supported by GROW, the Dutch Cancer Society KWF (UM2009-4352), and the Association for International Cancer Research, AICR (11-0678). SD is supported by a GCU studentship and Patricia E. Martin is supported by a grant from Tenovus Scotland (S09/5).

REFERENCES

Abell E, Read SI (1980) Porokeratotic eccrine ostial and dermal duct naevus. *Br J Dermatol* 103:435–41

Aloi FG, Pippione M (1986) Porokeratotic eccrine ostial and dermal duct nevus. *Arch Dermatol* 122:892–5

Arita K, Akiyama M, Aizawa T *et al.* (2006) A novel N14Y mutation in Connexin26 in keratitis-ichthyosis-deafness syndrome: analyses of altered gap junctional communication and molecular structure of N terminus of mutated Connexin26. *Am J Pathol* 169:416–23

Bakirtzis G, Choudhry R, Aasen T *et al.* (2003) Targeted epidermal expression of mutant Connexin 26(D66H) mimics true Vohwinkel syndrome and provides a model for the pathogenesis of dominant connexin disorders. *Hum Mol Genet* 12:1737–44

Cambiaghi S, Gianotti R, Caputo R (2007) Widespread porokeratotic eccrine ostial and dermal duct nevus along Blaschko lines. *Pediatr Dermatol* 24:162–7

Cobb MW, Vidmar DA, Dilaimy MS (1990) Porokeratotic eccrine ostial and dermal duct nevus: a case of systematized involvement. *Cutis* 46: 495–7

Criscione V, Lachiewicz A, Robinson-Bostom L *et al.* (2010) Porokeratotic eccrine duct and hair follicle nevus (PEHFN) associated with keratitis-ichthyosis-deafness (KID) syndrome. *Pediatr Dermatol* 27:514–7

de Zwart-Storm EA, Hamm H, Stoevesandt J *et al.* (2007) A novel missense mutation in GJB2 disturbs gap junction protein transport and causes focal palmoplantar keratoderma with deafness. *J Med Genet* 45:161–6

de Zwart-Storm EA, Martin PE, Van Steensel MAM (2009) Gap junction diseases of the skin: novel insights from new mutations. *Expert Rev Dermatol* 4:455–68

de Zwart-Storm EA, Rosa RF, Martin PE *et al.* (2011) Molecular analysis of connexin26 asparagine14 mutations associated with syndromic skin phenotypes. *Exp Dermatol* 20:408–12

de Zwart-Storm EA, van Geel M, van Neer PA *et al.* (2008) A novel missense mutation in the second extracellular domain of GJB2, p.Ser183Phe, causes a syndrome of focal palmoplantar keratoderma with deafness. *Am J Pathol* 173:1113–9

Dürig J, Rosenthal C, Halfmeyer K *et al.* (2000) Intercellular communication between bone marrow stromal cells and CD34+ haematopoietic progenitor cells is mediated by connexin 43-type gap junctions. *Br J Haematol* 111:416–25

Easton JA, Petersen JS, Martin PE (2009) The anti-arrhythmic peptide AAP10 remodels Cx43 and Cx40 expression and function. *Naunyn Schmiedebergs Arch Pharmacol* 380(1):11–24

Goddard DS, Rogers M, Frieden IJ *et al.* (2009) Widespread porokeratotic adnexal ostial nevus: clinical features and proposal of a new name unifying porokeratotic eccrine ostial and dermal duct nevus and porokeratotic eccrine and hair follicle nevus. *J Am Acad Dermatol* 61:1060 e1–4

Happle R, Rogers M (2002) Epidermal nevi. *Adv Dermatol* 18:175–201

Jan AY, Amin S, Ratajczak P *et al.* (2004) Genetic heterogeneity of KID syndrome: identification of a Cx30 gene (GJB6) mutation in a patient with KID syndrome and congenital atrichia. *J Invest Dermatol* 122: 1108–13

Kroumpouzos G, Stefanato CM, Wilkel CS *et al.* (1999) Systematized porokeratotic eccrine and hair follicle naevus: report of a case and review of the literature. *Br J Dermatol* 141:1092–6

Lazic T, Li Q, Frank M *et al.* (2011) Extending the phenotypic spectrum of keratitis-ichthyosis-deafness syndrome: report of a patient with GJB2 (G12R) connexin 26 mutation and unusual clinical findings. *Pediatr Dermatol*; e-pub ahead of print 20 October 2011

Lee JR, Derosa AM, White TW (2009) Connexin mutations causing skin disease and deafness increase hemichannel activity and cell death when expressed in Xenopus oocytes. *J Invest Dermatol* 129:870–8

Leybaert L, Braet K, Vandamme W *et al.* (2003) Connexin channels, connexin mimetic peptides and ATP release. *Cell Commun Adhes* 10: 251–7

Marziano NK, Casalotti SO, Portelli AE *et al.* (2003) Mutations in the gene for connexin 26 (GJB2) that cause hearing loss have a dominant negative effect on connexin 30. *Hum Mol Genet* 12:805–12

Richard G, Rouan F, Willoughby CE *et al.* (2002) Missense mutations in GJB2 encoding connexin-26 cause the ectodermal dysplasia keratitis-ichthyosis-deafness syndrome. *Am J Hum Genet* 70(5):1341–8

Rouan F, White TW, Brown N *et al.* (2001) Trans-dominant inhibition of connexin-43 by mutant connexin-26: implications for dominant connexin disorders affecting epidermal differentiation. *J Cell Sci* 114: 2105–13

Rudkin GH, Carlsen BT, Chung CY *et al.* (2002) Retinoids inhibit squamous cell carcinoma growth and intercellular communication. *J Surg Res* 103:183–9

Sassmannshausen J, Bogomilsky J, Chaffins M (2000) Porokeratotic eccrine ostial and dermal duct nevus: a case report and review of the literature. *J Am Acad Dermatol* 43:364–7

Titeux M, Mendonca V, Decha A *et al.* (2009) Keratitis-ichthyosis-deafness syndrome caused by GJB2 maternal mosaicism. *J Invest Dermatol* 129:776–9

van Steensel M, van Geel M, Nahuys M *et al.* (2002) A novel connexin 26 mutation in a patient diagnosed with keratitis-ichthyosis-deafness syndrome. *J Invest Dermatol* 118:724–7

Wright CS, Pollok S, Flint DJ *et al.* (2012) The connexin mimetic peptide Gap27 increases human dermal fibroblast migration in hyperglycemic and hyperinsulinemic conditions *in vitro*. *J Cell Physiol* 227:77–87

Wu BL, Lindeman N, Lip V *et al.* (2002) Effectiveness of sequencing connexin 26 (GJB2) in cases of familial or sporadic childhood deafness referred for molecular diagnostic testing. *Genet Med* 4:279–88

Ziambaras K, Lecanda F, Steinberg TH *et al.* (1998) Cyclic stretch enhances gap junctional communication between osteoblastic cells. *J Bone Miner Res* 13:218–28